Supplementary

Polarity-Dependent Twisted Intramolecular Charge Transfer in Diethylamino Coumarin Revealed by Ultrafast Spectroscopy

Jiawei Liu †, Cheng Chen † and Chong Fang *,‡

Department of Chemistry, Oregon State University, 153 Gilbert Hall, Corvallis, OR 97331, USA
* Correspondence: chong.fang@oregonstate.edu; Tel.: +1-541-737-6704
† These authors contributed equally to this work.
‡ Web: https://fanglab.oregonstate.edu/.

Table of Contents

1. Supplementary Figures

Figure S1. Semilogarithmic contour plots of fs-TA spectra for coumarin 481 (C481) in 14 solvents after 400 nm excitation……..…S2
Figure S2. Global analysis of fs-TA spectra for C481 in 14 different solvents…….S3
Figure S3. HOMO and LUMO electron density distributions with energies for FS and TICT states of C481 in three solvents with decreasing polarity…… S3
Figure S4. The experimental and calculated ground-state Raman spectra of C481 in three solvents with decreasing polarity……..…S4
Figure S5. Representative FSRS traces with spectral baselines of C481 in MeOH, DMSO, and Toluene ……...…..…S5

2. Supplementary Tables

Table S1. Photophysical and solvent properties of C481 in various solvents…….... S6
Table S2. Multivariable regression of nonradiative decay rate constant and ratio of nonradiative over radiative decay rate constant for C481…….…… S7
Table S3. Kamlet–Taft analysis for absorption and emission of C481…….……S8
Table S4. Ground state Raman mode assignments for C481 in three solvents with decreasing polarity……...……S8
Table S5. Ground (GS, S_0) and excited state (ES, S_1) Raman marker band for C481 in different solvents with decreasing polarity……..... S9
Table S6. Calculations with dispersion correction and explicit solvent……..... S9

3. Supplementary References……..……S10

1. Supplementary Figures

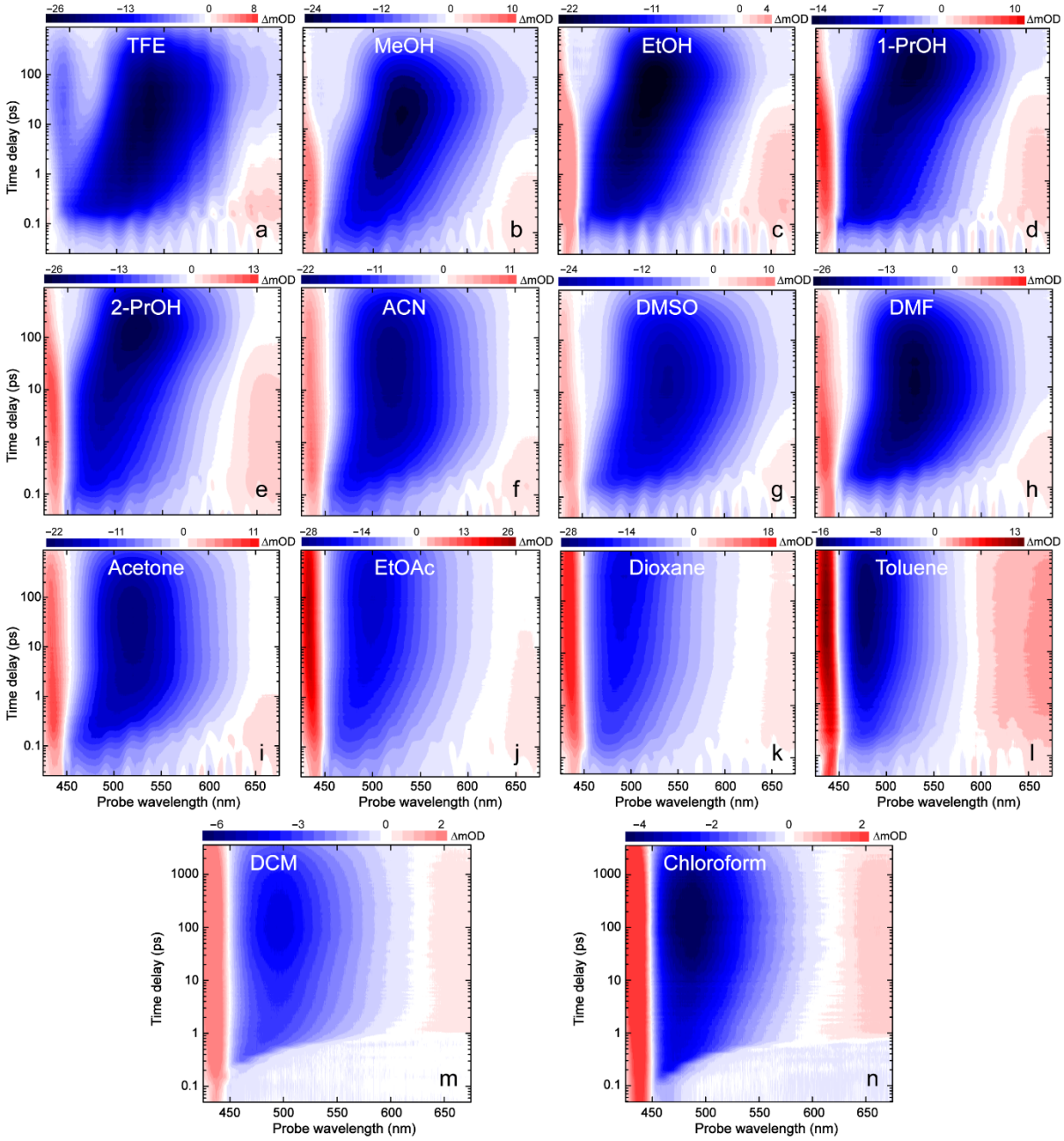

Figure S1. Semilogarithmic contour plots of fs-TA spectra for coumarin 481 (C481) in 14 solvents after 400 nm excitation. (**a**)-(**l**) Experimental TA spectra collected within a time window of ~900 ps. Due to an apparently long and rather flat SE band decay within 900 ps in (**m**) DCM and (**n**) chloroform, a separate TA setup with ~3.6 ns time window was used. The solvent used is denoted in each panel, and the signal intensity is reflected by the horizontal color bar (blue: negative; red: positive) in milli-optical-density (mOD) unit above each panel.

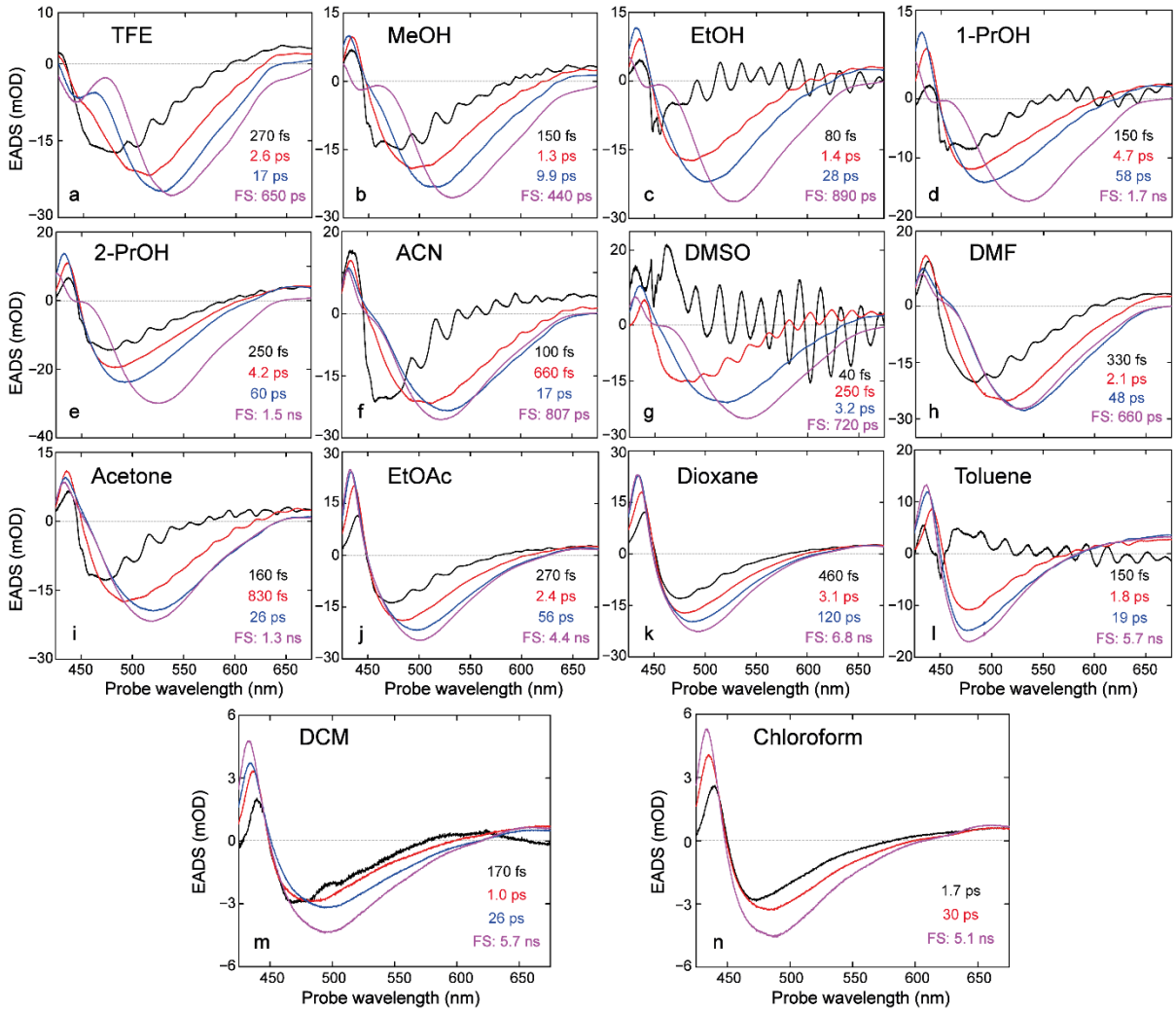

Figure S2. Global analysis of fs-TA spectra for C481 in 14 different solvents after 400 nm excitation. The sequential kinetic scheme of pertinent electronic dynamics is indicated by the evolution-associated difference spectra (EADS) plot in each solvent (denoted in panels **a**-**n**). The retrieved lifetimes in association with transient electronic species are in the order of black→red(→blue)→magenta, with the absence of blue component only in chloroform (panel **n**). The florescent state (FS) lifetime is bolded in the inset of each panel.

Notably, the spectral modulations mostly visible in the fastest component (sub-ps timescale, see black traces in panels **a**-**l**) may involve Franck–Condon relaxation and/or the initial solvation process [1,2], which are neither spectrally separable from time-resolved electronic data [3] nor central to our discussion on the chromophore fluorogenicity in solution [4].

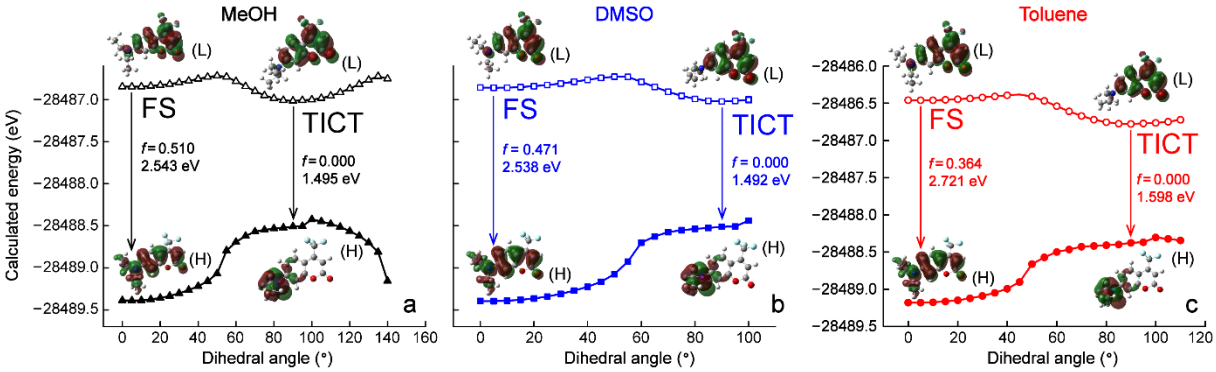

Figure S3. Calculated HOMO and LUMO electron density distributions with energies for FS and TICT states of C481 in three representative solvents with decreasing polarity (MeOH > DMSO >

Toluene). The dihedral angle was scanned across the possible twisting range of the diethylamino group, and the calculated energy values are shown in hollow (excited state, S_1) and solid (ground state, S_0) black triangles, blue squares, and red circles for C481 in (**a**) MeOH, (**b**) DMSO, and (**c**) Toluene, respectively. The HOMO–LUMO energy gap (in eV unit) and transition oscillator strength (*f*) are labeled by each vertical downward transition, positioned near the optimized dihedral angles corresponding to the excited-state local energy minima at the FS and TICT states. (H) and (L) denote HOMO and LUMO, respectively. See Table S6 below for supplementary calculations with dispersion correction [5-7] to corroborate the usefulness of these economical DFT calculations depicted herein to capture the photoresponse of such organic chromophores in solution [8].

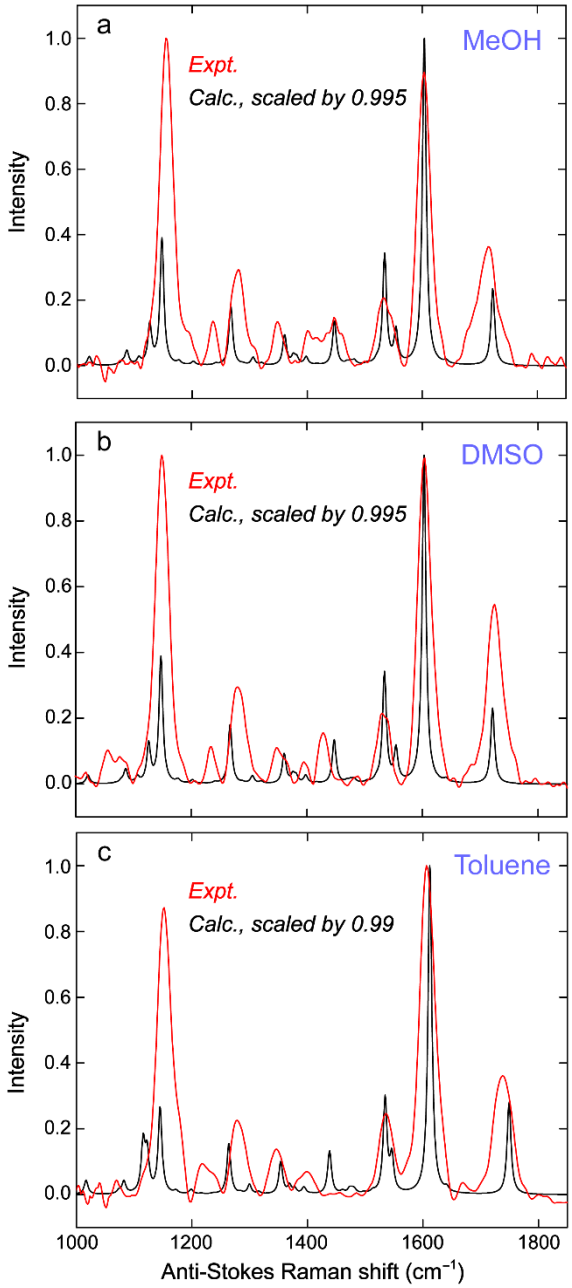

Figure S4. The experimental (red) and calculated (blue) ground state (S_0) Raman spectra of C481 in various solvents with decreasing polarity (MeOH > DMSO > Toluene) as retrieved from the GS-FSRS measurements and DFT-B3LYP calculations. The Raman pump wavelength in FSRS was tuned to 540 nm for C481 in (**a**) MeOH and (**b**) DMSO, as well as 498 nm in (**c**) Toluene, to achieve the desirable pre-resonance conditions. The frequency scaling factors (i.e., 0.995 for C481 in both MeOH and DMSO, and 0.99 for C481 in toluene) to match the calculated (black) and experimental (red) spectra are listed in each panel. The Raman spectra are normalized in the spectral region, and the stimulated Raman signal intensity (red) and anti-Stokes Raman shift axis are both multiplied by –1 for a better visual comparison in each panel.

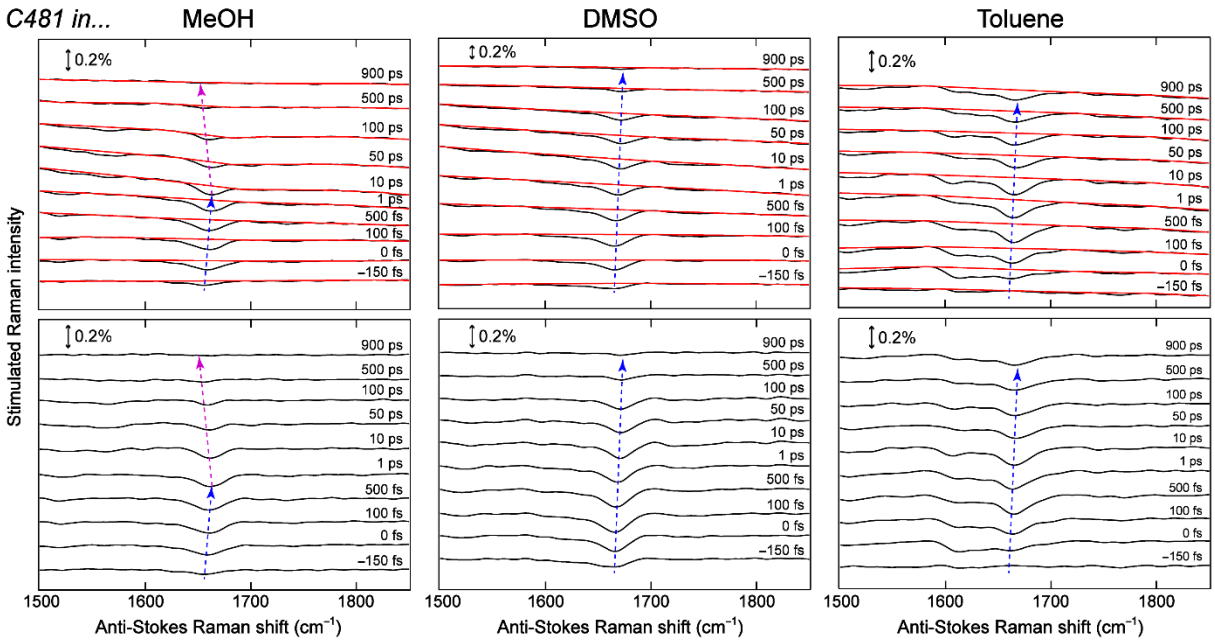

Figure S5. Representative FSRS traces with spectral baselines of C481 in MeOH (left), DMSO (middle), and Toluene (right panels) after 400 nm excitation. The raw experimental spectra collected and smooth spline baselines drawn are colored in black and red, respectively, in the top three panels. The corresponding bottom panels display the pure excited-state spectra (black) after baseline subtractions. The selected ten time delay points across the detection time window are shown above the associated experimental spectra. Blue and magenta dashed lines indicate the Raman marker band (C=O stretch) peak frequency blueshift and redshift, respectively, with time in the electronic excited state (see Figure 4f in main text). The double-headed arrow in each panel denotes the stimulated Raman intensity (loss) magnitude of 0.2%.

2. Supplementary Tables

Table S1. Photophysical properties of C481 in various solvents.

Solvent	Relative Polarity (E_T^N)	Solvent Properties				τ_{FS} (ns) [a]	k_r ($\times 10^8$ s^{-1}) [b]	k_{nr} ($\times 10^8$ s^{-1}) [b]
		α	β	π*	η (cp)			
TFE	0.898	1.51	0	0.73	1.75	0.65	0.97	14
MeOH [c]	0.762	0.93	0.62	0.60	0.59	0.44	0.98	22
EtOH	0.654	0.83	0.77	0.54	1.10	0.89	0.97	10
1-PrOH	0.617	0.84	0.90	0.52	2.26	1.7	0.90	5.1
2-PrOH	0.546	0.76	0.95	0.48	2.40	1.5	1.2	5.5
ACN	0.460	0.19	0.31	0.75	0.38	0.81	1.0	11
DMSO [c]	0.444	0	0.76	1.00	2.00	0.72	0.99	13
DMF	0.386	0	0.69	0.88	0.92	0.66	1.1	14
Acetone	0.355	0.08	0.48	0.71	0.36	1.3	1.1	6.6
DCM	0.309	0.30	0	0.73	0.44	5.7	1.5	0.26
$CHCl_3$	0.259	0.44	0	0.58	0.57	5.1	1.7	0.24
EtOAc	0.228	0	0.45	0.55	0.45	4.4	1.7	0.55
Dioxane	0.164	0	0.37	0.55	1.37	6.8	1.2	0.24
Toluene [c]	0.099	0	0.11	0.54	0.56	5.7	1.5	0.26

[a] The fluorescent state (FS) lifetime was retrieved from fs-TA spectral data with global analysis (Figures S1 and S2). Two significant figures are consistently kept for the time constants and rate constants in this table.

[b] Radiative (k_r) and nonradiative (k_{nr}) decay rate constants were calculated using Equations (3) and (4) (see main text) with the experimental values of k_{FS} (i.e., $\frac{1}{\tau_{FS}}$) and ϕ (i.e., FQY). The base 10 logarithmic plots of k_{nr} vs. solvent polarity (E_T^N) can be found in Figure 2i for C481 across 14 solvents. Besides the largely invariant nature of k_r (0.9–1.7 $\times 10^8$ s^{-1} in our series, which nicely matches the reported common value of 1.5×10^8 s^{-1} in literature on 7-aminocoumarins [9,10] and the at most two-fold reduction in k_r in most polar solvents), the significant decrease of k_{nr} is highlighted by light gray shades for low-polarity solvents used (from DCM to Toluene; representing as much as two orders of magnitude decrease from the values in polar media), which plays a dominant role in the increased FQYs of C481 in nonpolar media (see Figure 1 and Table 1 in main text). Further support can be found in a previous report studying the emission properties of C481 in $CHCl_3$, showing a Stokes shift of 3673 cm^{-1}, fluorescence lifetime of 4.9 ns, and radiative lifetime of 7.9 ns ($k_r \approx 1.3 \times 10^8$ s^{-1}) [11], mostly matching our data in Table 1 (main text) and Table S1 above. Recently, more numerical values were reported for C481 in bulk MeOH using time-resolved fluorescence spectroscopy after 405 nm excitation [12], showing the fluorescence lifetime of 0.48 ns, FQY of 0.04, $k_r \approx 0.84 \times 10^8$ s^{-1} and $k_{nr} \approx 20 \times 10^8$ s^{-1}, all within 15% of the values we derived and tabulated in this work (see Table 1, Table S1, and Figure S2).

[b] The rate constants for radiative (k_r) and nonradiative (k_{nr}) decay rate constants have been reported for C481 in a few solvents [10], and the corresponding numerical values in ethyl acetate (EtOAc) are 2.4×10^8 s^{-1} and $<0.1\times 10^8$ s^{-1}, respectively, largely consistent with our results showing the much smaller k_{nr} in low-polarity solvents (highlighted by gray shades in Table S1). The reported values in acetonitrile (ACN) are 1.5 and 15 $\times 10^8$ s^{-1}, similar to our values of 1.0 and 11×10^8 s^{-1}. In high-polarity solvents like ethanol (EtOH), the reported values are 1.1 and 11 $\times 10^8$ s^{-1}, similar to our values of 0.97 and 10×10^8 s^{-1}. The consistent trend for these solvent-dependent rate constants lends further support to such a systematic analysis of fs-TA spectra in delineating the molecular origin for the significant fluorogenicity of C481 with the bulky and free-rotor diethylamino substituent [4,10,13,14].

[c] There is a correlation of the Stokes shift (Table 1) with the nonradiative decay rate (Table S1) for three representative solvents (MeOH > DMSO > Toluene, in the order of polarity): 5340 > 4910 > 3660 cm^{-1} Stokes shift values in comparison with 22 > 13 > 0.26 $\times 10^8$ s^{-1} k_{nr} values. This trend likely reflects a reduction of nonradiative decay in low-polarity solvents with an increased FS (ICT) → TICT transition state energy barrier (Figure 3) [4,10]. In essence, the Stokes shift can serve as an indicator for the CT nature of the transition and the probability to cross over the FS→TICT energy barrier [10], so a larger Stokes shift is in accord with an more efficient arrival at the twisted, low-oscillator strength TICT state along with an effective FQY reduction (due to less FS population) in high-polarity solvents like MeOH.

Table S2. Multivariable regression of nonradiative decay rate constant and ratio of nonradiative over radiative decay rate constants for C481 in solution.

Compound	coeff. [a]	$\log(k_{nr})$			$\log(\frac{1}{\phi}-1)$		
		value	p-value [b]	R^2	value	p-value [b]	R^2
C481	a	1.24	0.0004	0.88	1.36	0.0006	0.88
	b	1.71	0.0004		1.87	0.0005	
	p	3.09	0.0008		3.40	0.001	
	$\log(k_0)$ [c]	5.05	3×10^{-6}		–3.35	0.0002	
	δ [d]	0.98	0.031		0.99	0.048	

[a] The pertinent equations for $\log(k_{nr})$ and $\log(\frac{1}{\phi}-1)$ can be found as Equations (6) and (8) in main text, respectively. The pertinent data plots against solvent polarity (E_T^N) are displayed in Figure 2i,j for C481 across 14 solvents.

[b] The retrieved coefficients from multivariable linear regression are all statistically significant (p < 0.05, at the 95% confidence level) in this table.

[c] This quantity changes to $\log(k_0/k_r)$ when performing the multivariable analysis of $\log(\frac{1}{\phi}-1)$. See Table S1 for the largely invariant k_r values and main text Section 3.2 for more discussions about the comparative linear regression results listed in this table.

[d] The associated p-values are the largest for solvent viscosity parameter, meaning that the coefficient δ becomes statistically insignificant at the 97% confidence level. Overall, the solvent polarity parameters are statistically more significant in this table.

Table S3. Kamlet–Taft analysis for absorption and emission peaks of C481.

Compound	coeff. [a]	Absorption			Emission		
		value [b]	p-value [b]	R^2	value	p-value	R^2
C481	a	–0.718	1.4×10^{-6}	0.93	–1.26	1.4×10^{-5}	0.92
	b	–0.079	0.43		–1.28	0.0001	
	p	–1.91	6.6×10^{-6}		–3.24	7.6×10^{-5}	
	$\tilde{\nu}_0$	26.6	2.4×10^{-18}		23.7	2.5×10^{-14}	

[a] The spectral value $\tilde{\nu}$ (absorption or emission peak), fit intercept $\tilde{\nu}_0$ (peak frequency in the absence of solvent), and all the coefficients have 10^3 cm^{-1} unit. The equation used is $\tilde{\nu} = \tilde{\nu}_0 + a\alpha + b\beta + p\pi^*$ [4,15]. The solvent polarity parameters (α, β, and π^*) are listed in Table S1.

[b] The statistically insignificant coefficients ($p > 0.05$, at the 95% confidence level) for the absorption peaks of C481 in various solvents are highlighted by light gray shades.

Notably, the steady-state electronic absorption peak of C481 shows a prominent dependence on the solvent H-bond donating capability (α) and dipolarity (π^*) of solvent molecule (Table 1 and Table S1) [11]. Both the retrieved coefficients for α and π^* are negative, indicating that the H-bond accepting capability and dipole moment of the chromophore increases from S_0 to S_1, which stabilizes S_1 more than S_0 and results in a reduced absorption energy gap in solvents with increasing polarity. The insignificant contribution from the solvent H-bond accepting capability (β) is in accord with the chemical structure of C481 (see Scheme 1) that lacks a dissociable proton and H-bond donating capability in general, while the diethylamino group lacks any amino hydrogens that can potentially act as a H-bond donor to the solvent [11].

Meanwhile, the steady-state electronic emission peak of C481 shows both solvent H-bond donating (α) and accepting (β) capabilities as well as dipolarity (π^*) contribute to the emission energy gap. All the coefficients remain negative and acquire a larger magnitude than those from the absorption fits, in accord with a prominent intramolecular charge transfer (ICT) following photoexcitation of C481 [10,11]. Meanwhile, the negative coefficient for β (with a statistically significant value since $p < 0.05$) indicates that the H-bond donating capability of the chromophore increases from S_0 to S_1 (at the relaxed S_1 geometry), likely due to the excited-state ICT and associated electrostatic effects that involve specific solute-solvent interactions (not directly in relation to an explicit dissociable proton, see more discussions in main text).

Table S4. Ground state Raman mode assignments for C481 in various solvents.

Exp. Freq. (cm^{-1}) [a]			Cal. Freq. (cm^{-1}) [b]			
MeOH	DMSO	Toluene	MeOH	DMSO	Toluene	Vibrational mode assignments (major)
1154	1150	1152	1147	1147	1145	Benzene ring-H scissoring, benzene ring and pyran ring in-plane deformation, C–C, C–O, and C–F stretch
1281	1280	1277	1267	1267	1264	C–C(F_3) stretch, pyran C–H rocking, with benzene ring-H rocking
1349	1347	1346	1361	1361	1354	Benzene ring in-plane deformation, diethylamino C–H rocking
1532	1530	1535	1535	1534	1534	Benzene ring and pyran ring C=C stretch, diethylamino C–H bending
1603	1603	1606	1603	1603	1612	Pyran and benzene ring C=C stretch
1714	1724	1737	1722	1723	1749	C=O stretch, pyran and benzene ring C=C stretch

[a] The experimental ground state (S_0) Raman mode frequencies of C481 in three representative solvents were retrieved from the GS-FSRS spectral data in Figure 4a (see main text).

[b] The ground state Raman mode frequencies were calculated using Gaussian 16 software and density functional theory (DFT) at the B3LYP level with 6-311G+(d,p) basis sets for the geometrically optimized chromophore structure in various solvents (see Figure 3 for the output frontier molecular orbitals with electron density distributions, and Scheme 1 for the C481 chemical structure). The calculated vibrational normal mode frequencies are scaled by a factor of 0.995 for both MeOH and DMSO cases (Figure S4a,b) and 0.99 for Toluene (Figure S4c). The general trend of experimental Raman mode frequency change from MeOH, DMSO, to Toluene (e.g., a redshift of the 1281, 1349

cm^{-1} modes and a blueshift of the 1603, 1714 cm^{-1} modes) was captured by DFT calculations, validating the systematic analysis and vibrational mode assignments with economical quantum calculations (see Section 2.5 in main text for methods, and supplementary calculations below listed in Table S6) for C481 in various solvents.

Table S5. Ground (GS, S_0) and excited state (ES, S_1) Raman marker band for C481 in three solvents with decreasing polarity.

Solvent	GS Freq. (cm^{-1}) [a]	ES Freq. (cm^{-1}) [a]	Calc. ES Freq. (cm^{-1}) [b]	Vibrational Mode Assignments (major)
MeOH	1714	1658	1662	C=O and C=C stretch on pyran ring
DMSO	1724	1667	1661	
Toluene	1737	1657	1697	

[a] As the C=O group on pyran ring of C481 exhibits pronounced solvent dependence with a largely localized contribution, we selected this Raman marker band (C=O along with C=C stretch) using FSRS to study the frequency trend. From S_0 to S_1, this vibrational mode promptly displays a pronounced redshift in all solvents studied (~56, 57, and 80 cm^{-1} in MeOH, DMSO, and Toluene, respectively). Subsequently in S_1, the C=O stretching mode starts to blue-shift as expected for a sensitive local probe undergoing vibrational cooling during the chromophore's excited-state relaxation [2,16,17]. In difference from a continuous frequency blueshift in both DMSO and Toluene, this Raman marker band of C481 in MeOH displays a notable redshift after ~2 ps (Figure 4f), likely due to the relatively strong H-bonding network in high-polarity protic solvents (such as MeOH) that rearranges on the ps timescale prior to fluorescence [2,18]. In particular, the re-establishment of optimal H-bonding interactions at the pyran-ring C=O end as the photoexcited C481 undergoes energy dissipation from FS toward TICT state and ground state (see Figure 3 in main text) results in the observed C=O stretching frequency redshift (also affecting the C=C stretch via electrostatic interactions/conjugation and electron redistribution over the molecular framework of C481).

[b] The excited state vibrational frequency for this normal mode was calculated in the Gaussian 16 software [7] using time-dependent (TD)-DFT at B3LYP level with 6-311G+(d,p) basis sets for the geometrically optimized excited-state chromophore structure in various solvents. A frequency scaling factor of 0.97 was applied to compare the calculated value to the experimental value, and the deviation likely arises from the limitation of TD-DFT calculations for molecular systems capable of prominent ICT and subject to specific H-bonding interactions with the surrounding solvent molecules [2,19]. The simultaneous match between the observed and calculated GS as well as ES Raman peaks confirms the C=O/C=C stretch mode assignment for C481 in solution.

Table S6. Quantum (TD-DFT) calculation results with dispersion correction and an explicit solvent molecule for C481 in MeOH.

	Expt.	Calc. [a]			
		implicit [b], no DC	implicit [b], DC	explicit [c], no DC	explicit [c], DC
λ_{abs} (nm)	402	405	405	411	411
TS barrier (eV) [d]	–	0.13	0.13	–	–

[a] Dispersion correction (DC) was performed using Grimme's dispersion with the original D_3 damping function (GD3) [5,7]. TD-DFT calculations were employed to yield the energy gaps between the electronic ground (S_0) and excited (S_1) states for C481 in solution.

[b] The bulk solvent effect was incorporated via the implicit integral equation formalism variant polarizable continuum model (IEFPCM) in Gaussian 16 software [7].

[c] The one "explicit" protic solvent molecule (MeOH here) was added (in proximity to the C=O group of C481, the optimized O···O distance was 2.73 Å that is a typical H-bond length) with bulk solvent still modelled by IEFPCM, demonstrated to yield useful results for explicit H-bonded molecules in solution [20]. A single-point excited-state energy calculation at FS (~5° dihedral angle) using TD-DFT with an explicit MeOH molecule plus IEFPCM yields a S_1-S_0 energy gap of 2.502 eV, close to 2.543 eV with implicit solvent only (see Figure S3a above).

[d] The FS-to-TICT barrier height was calculated by the energy difference between the transition state (TS) which we took the dihedral angle of 50° as a close approximation (see Figure S3 above for the reaction coordinate scan and the apparent barrier location) and the FS minimum (dihedral angle of ~5°). For further corroboration, we also calculated the energy difference between FS minimum and TS peak region at the adjacent dihedral angles of 45° and 55°. The corresponding implicit/no DC and implicit/DC barrier heights are 0.12 and 0.11 eV for FS-to-TS (45°), respectively, and 0.12 and

0.098 eV for FS-to-TS (55°), so the TS peak location at the dihedral angle of 50° still holds with dispersion correction. All these calculations show that the dispersion correction plays a minor role in affecting the excited-state TS barrier height by scanning the dominant diethylamino group dihedral angle (i.e., between the coumarin backbone and one arm of the $–NEt_2$ group, see Scheme 1 left panel in main text) from the FS toward the lower-lying TICT state (see Figure S3 for C481 in three representative solvents).

3. Supplementary References

1. Berera, R.; van Grondelle, R.; Kennis, J.M. Ultrafast transient absorption spectroscopy: Principles and application to photosynthetic systems. *Photosynth. Res.* **2009**, *101*, 105-118.
2. Fang, C.; Tang, L.; Chen, C. Unveiling coupled electronic and vibrational motions of chromophores in condensed phases. *J. Chem. Phys.* **2019**, *151*, 200901.
3. Chen, C.; Tutol, J.N.; Tang, L.; Zhu, L.; Ong, W.S.Y.; Dodani, S.; Fang, C. Excitation ratiometric chloride sensing in a standalone yellow fluorescent protein is powered by the interplay between proton transfer and conformational reorganization. *Chem. Sci.* **2021**, *12*, 11382–11393.
4. Chen, C.; Boulanger, S.A.; Sokolov, A.I.; Baranov, M.S.; Fang, C. A novel dialkylamino GFP chromophore as an environment-polarity sensor reveals the role of twisted intramolecular charge transfer. *Chemosensors* **2021**, *9*, 234.
5. Grimme, S.; Antony, J.; Ehrlich, S.; Krieg, H. A consistent and accurate *ab initio* parametrization of density functional dispersion correction (DFT-D) for the 94 elements H-Pu. *J. Chem. Phys.* **2010**, *132*, 154104.
6. Korth, M.; Pitoňák, M.; Řezáč, J.; Hobza, P. A transferable H-bonding correction for semiempirical quantum-chemical methods. *J. Chem. Theory Comput.* **2010**, *6*, 344-352.
7. Frisch, M.J.; Trucks, G.W.; Schlegel, H.B.; Scuseria, G.E.; Robb, M.A.; Cheeseman, J.R.; Scalmani, G.; Barone, V.; Petersson, G.A.; Nakatsuji, H.*, et al. Gaussian 16, Revision C.01*, Gaussian, Inc.: Wallingford, CT, 2016.
8. Boulanger, S.A.; Chen, C.; Myasnyanko, I.N.; Sokolov, A.I.; Baranov, M.S.; Fang, C. Excited-state dynamics of a *meta*-dimethylamino locked GFP chromophore as a fluorescence turn-on water sensor. *Photochem. Photobiol.* **2022**, *98*, 311-324.
9. Jones, G., II; Jackson, W.R.; Halpern, A.M. Medium effects on fluorescence quantum yields and lifetimes for coumarin laser dyes. *Chem. Phys. Lett.* **1980**, *72*, 391-395.
10. Jones, G.; Jackson, W.R.; Choi, C.Y.; Bergmark, W.R. Solvent effects on emission yield and lifetime for coumarin laser dyes. Requirements for a rotatory decay mechanism. *J. Phys. Chem.* **1985**, *89*, 294-300.
11. Das, K.; Jain, B.; Patel, H.S. Hydrogen bonding properties of coumarin 151, 500, and 35: The effect of substitution at the 7-amino position. *J. Phys. Chem. A* **2006**, *110*, 1698-1704.
12. Shabbir, A.; Jang, T.; Lee, G.; Pang, Y. Intramolecular charge transfer of coumarin dyes confined in *methanol-in-oil* reverse micelles. *J. Mol. Liq.* **2022**, *346*, 118313.
13. Litvinenko, K.L.; Webber, N.M.; Meech, S.R. Internal conversion in the chromophore of the green fluorescent protein: Temperature dependence and isoviscosity analysis. *J. Phys. Chem. A* **2003**, *107*, 2616-2623.
14. Amdursky, N.; Erez, Y.; Huppert, D. Molecular rotors: What lies behind the high sensitivity of the thioflavin-T fluorescent marker. *Acc. Chem. Res.* **2012**, *45*, 1548-1557.
15. Kamlet, M.J.; Abboud, J.-L.M.; Abraham, M.H.; Taft, R.W. Linear solvation energy relationships. 23. A comprehensive collection of the solvatochromic parameters, π*, α, and β, and some methods for simplifying the generalized solvatochromic equation. *J. Org. Chem.* **1983**, *48*, 2877-2887.
16. Nibbering, E.T.J.; Fidder, H.; Pines, E. Ultrafast chemistry: Using time-resolved vibrational spectroscopy for interrogation of structural dynamics. *Annu. Rev. Phys. Chem.* **2005**, *56*, 337-367.
17. Tang, L.; Wang, Y.; Zhu, L.; Lee, C.; Fang, C. Correlated molecular structural motions for photoprotection after deep-UV irradiation. *J. Phys. Chem. Lett.* **2018**, *9*, 2311-2319.
18. Bakker, H.J. Structural dynamics of aqueous salt solutions. *Chem. Rev.* **2008**, *108*, 1456-1473.
19. Rohrdanz, M.A.; Martins, K.M.; Herbert, J.M. A long-range-corrected density functional that performs well for both ground-state properties and time-dependent density functional theory excitation energies, including charge-transfer excited states. *J. Chem. Phys.* **2009**, *130*, 054112.
20. Mennucci, B. Hydrogen bond versus polar effects: An ab initio analysis on n → π* absorption spectra and N nuclear shieldings of diazines in solution. *J. Am. Chem. Soc.* **2002**, *124*, 1506-1515.